Carcinogenesis vol.22 no.8 pp.1139–1148, 2001

Cerivastatin, an inhibitor of HMG-CoA reductase, inhibits the signaling pathways involved in the invasiveness and metastatic properties of highly invasive breast cancer cell lines: an *in vitro* study

Christophe Denoyelle[1], Marc Vasse[1], Marie Körner[2], Zohair Mishal[3], Florence Ganné[1], Jean-Pierre Vannier[1], Jeannette Soria[4] and Claudine Soria[1,5,6]

[1]Laboratoire DIFEMA, Groupe de Recherche MERCI, UFR de Médecine et de Pharmacie, Rouen, [2]CNRS, UPR 9079, Institut André Lwoff, Villejuif, [3]CNRS, IFR 2249, Villejuif, [4]Laboratoire de Biochimie Sainte Marie, Hôtel Dieu de Paris, Paris and [5]INSERM U353, Hôpital St Louis, Paris, France

[6]To whom correspondence should be addressed at: Groupe de Recherche MERCI, Laboratoire DIFEMA, UFR de Médecine et Pharmacie, 22 Boulevard Gambetta, 76183 Rouen Cedex, France

Cerivastatin is used in the treatment of hypercholesterolemia to inhibit 3-hydroxy 3-methylglutaryl coenzyme A reductase and thus prevent the synthesis of cholesterol precursors, such as farnesyl pyrophosphate (FPP) and geranylgeranyl pyrophosphate (GGPP), responsible, respectively, for translocation of Ras and Rho to the cell membrane, a step required for their cell signaling, leading to cell proliferation and migration. Recently, it has been suggested that non lipid-related effects of statins could play a beneficial role in cancer therapy. In this study, we have investigated the mechanisms by which statins inhibit cancer and the types of cancers which could benefit from this therapy. In MDA-MB-231 cells, an aggressive breast cancer cell line with spontaneous activation of Ras and NFκB and overexpression of RhoA, cerivastatin induced inhibition of both cell proliferation and invasion through Matrigel. This anti-proliferative effect was related to G_1/S arrest due to an increase in $p21^{Waf1/Cip1}$. The anti-invasive effect was observed from 18 h and could be explained by RhoA delocalization from the cell membrane, resulting in disorganization of the actin fibers and disappearance of focal adhesion sites. The importance of RhoA inactivation in both these inhibitory effects was proved by their reversion by GGPP but not by FPP. Moreover, cerivastatin was also shown to induce inactivation of NFκB, in a RhoA inhibition-dependent manner, resulting in a decrease in urokinase and metalloproteinase-9 expression, two proteases involved in cell migration. The participation of Ras inactivation is considered a subsidiary mechanism for the effects of cerivastatin, as they were not rescued by FPP. Prolonged treatment of MDA-MB-231 cells with high doses of cerivastatin induced a loss of cell attachment. Interestingly, the effect of cerivastatin was considerably lower on poorly invasive MCF-7 cells. In conclusion, our results suggest that cerivastatin inhibits cell signaling pathways involved in the invasiveness and metastatic properties of highly invasive cancers.

Abbreviations: BSA, bovine serum albumin; cdki, cyclin-dependent kinase inhibitor; ELISA, enzyme-linked immunosorbent assay; EMSA, electrophoretic mobility shift assay; FITC, fluorescein isothiocyanate; FPP, farnesyl pyrophosphate; GGPP, geranylgeranyl pyrophosphate; HMG-CoA, 3-hydroxy 3-methylglutaryl coenzyme A; IκB, inhibitor κB; MAPK, mitogen-activated protein kinase; MMP-9, metalloproteinase-9; MVA, mevalonate; NFκB, nuclear factor κB; PBS, phosphate-buffered saline; TF, tissue factor; TNF-α, tumor necrosis factor α; u-PA, urokinase typeplasminogen.

Introduction

3-Hydroxy 3-methylglutaryl coenzyme A (HMG-CoA) reductase inhibitors (statins) are currently used in the treatment of hypercholesterolemia to prevent the transformation of HMG-CoA to mevalonate (MVA), a precursor of cholesterol synthesis. However, it has recently been suggested that non-lipid-related effects of statins could play a potentially beneficial role in cancer therapy (1). In experimental models, statin treatment was shown to diminish the growth of fibrosarcomas and experimental lung metastases in rats (2). Moreover, in a major clinical trial simvastatin, was shown to have cancer prevention capabilities (3). However, in this series the differences between the placebo and simvastatin groups were not markedly significant; this could be due to the fact that the patients included in the study were initially enrolled to assess the beneficial effects of a decrease in cholesterol and possible side effects. Therefore, although these authors demonstrated that simvastatin treatment reduced cancer mortality, they did not differentiate between the various types of cancers. In fact, some cancers may be more sensitive to this therapy.

The aim of our study was to investigate which types of cancers could benefit from this therapy and to evaluate the mechanisms by which statins inhibit cancer cell proliferation and/or invasiveness. The favorable effect induced by statins could be related to a decrease in the production of MVA derivatives, in particular farnesyl pyrophosphate (FPP) and geranylgeranyl pyrophosphate (GGPP). These isoprenoids are responsible for Ras and Rho prenylation, a step required for their translocation to the cell membrane, necessary for cell signaling (4). Farnesylation is required for correct localization of Ras, while the geranylgeranyl group is mostly involved in RhoA translocation to the cell membrane. In addition Ras, as well as RhoA, have been reported to play a significant role in the metastatic behavior of tumor cells (5).

Therefore, in this study we have analyzed the contribution of Ras and RhoA inhibition induced by cerivastatin (a potent HMG-CoA reductase inhibitor) on inhibition of both proliferation and invasiveness of a highly invasive and metastatic breast cancer cell line, MDA-MB-231, characterized by constitutive activation of Ras (6) and overexpression of RhoA (7). The effects of cerivastatin were also compared in MCF-7 cells, a poorly invasive and non-metastatic breast cancer cell line.

Initially we addressed the question of RhoA inhibition in cerivastatin anti-cancer activity. Indeed, a recent report has shown that RhoA prenylation is required for cell growth by suppressing $p21^{Waf1/Cip1}$ transcription (8). Furthermore, RhoA plays a role in cell invasiveness both by increasing cell motility (9) and by increasing AP-1 transcription (10).

Subsequently we analyzed the participation of Ras inhibition in the anti-proliferative effect of cerivastatin in the two cancer

cell lines. Indeed, Ras activates mitogen-activated protein kinase (MAPK), an important cell growth pathway (11).

Finally, because RhoA as well as oncogenic Ras enhance nuclear factor κB (NFκB) transcriptional activity (12,13), we also focused our attention on the effect of cerivastatin on NFκB activity, for the following reasons. Firstly, constitutive NFκB activation was found in some malignant phenotypes and contributes to cancer aggressivity. Indeed, in breast cancer it was found to be activated in highly metastatic MDA-MB-231 cells while it was not spontaneously activated in non-metastatic cells such as MCF-7 (14). Secondly, NFκB regulates the expression of many genes involved in cell invasiveness, such as urokinase type plasminogen (u-PA) (15), tissue factor (TF) (16) and metalloproteinase-9 (MMP-9) (17). In this respect, among the various enzyme systems expressed in cancer tissues, high levels of u-PA in breast cancer patients are associated with a poor prognosis (18), supporting the concept of the importance of these proteases in cell invasiveness (19,20). In addition to proteases, TF is also involved in intracellular signaling leading to metastasis and angiogenesis (21). Finally, NFκB is required for prevention of cell death induced by tumor necrosis factor α (TNF-α) and ionization radiation, since these factors alone are not effective in killing breast cancer cells which constitutively express activated NFκB (22–24).

Our study demonstrates that cerivastatin inhibits both proliferation and invasiveness of MDA-MB-231 cells, mainly by RhoA inhibition, whereas Ras was shown to play only a minimal role. Interestingly, the inhibitory activity of cerivastatin was much lower on MCF-7 cells. Consequently, these findings show that HMG-CoA inhibitors are most efficient in some types of particularly aggressive cancers and provide insights into the mechanism of inhibition of growth and invasion by these agents.

Materials and methods

Cell culture and reagents

Two human breast carcinoma cell lines, MDA-MB-231 and MCF-7, were used in this study. MDA-MB-231 cells were grown in RPMI 1640 medium (Eurobio, Les Ulis, France), while MCF-7 cells were cultured in Dulbecco's modified Eagle's medium (Eurobio). For both media 10% fetal calf serum (Costar, Brumath, France), 2 mM L-glutamine (Gibco BRL, New York, NY), 100 IU/ml penicillin (Sarbach, Suresnes, France), 100 μg/ml streptomycin (Diamant, Puteaux, France) were added. Cells were cultured at 37°C in a humidified 5% CO_2 atmosphere. Then adherent cells were incubated with cerivastatin sodium salt (Bayer) for different times in the presence or absence of MVA, FPP and GGPP at the indicated concentrations (Sigma, St Quentin Fallavier, France).

Cell proliferation assay

For the proliferation assay we used the minimal concentration of fetal calf serum (2%) to allow sufficient viability of MDA-MB-231 and MCF-7 cells. Briefly, after trypsinization the cells were seeded at a concentration of 5×10^4 cells/well in a 24-well plate (Costar, Cambridge, MA) and incubated with cerivastatin. Cell number was measured on day 3 for MDA-MB-231 and on day 5 for MCF-7 with a particle counter (Coulter Z1; Coultronics, France) after detachment with a non-enzymatic cell dissociation solution (Sigma). For MCF-7 cells the medium was renewed on day 3.

Apoptosis analysis

Phosphatidylserine expression on the surface of breast cancer lines

Annexin V binding and propidium iodide incorporation were analyzed using a commercial kit (Immunotech, Marseille, France) according to the manufacturer's instructions. Briefly, cells were washed in phosphate-buffered saline (PBS) and incubated for 15 min at 4°C with 10 μl of fluorescein isothiocyanate (FITC)-conjugated annexin V. Staining with propidium iodide (0.3 μg/ml) was performed to confirm the absence of cell membrane permeability.

DNA fragmentation assay

Genomic DNA was isolated using the SV total RNA isolation system (Promega, Madison, WI) according to the manufacturer's instructions with minor protocol modifications. The modifications involved a modified wash solution (70% ethanol) as well as digestion of the captured nucleic acids with 4 mg/ml RNase A (Boehringer, Mannheim, Germany) in yellow core buffer. After DNA elution all DNA samples were precipitated with 0.1 vol 3 M sodium acetate, pH 5.3, and 2 vol 100% ethanol, incubated overnight at –20°C, centrifuged for 10 min at 14 000 r.p.m. at room temperature and resuspended in 20 μl of nuclease-free water. An aliquot of each DNA sample was analyzed on a 2% agarose gel stained with ethidium bromide.

Cell cycle distribution using flow cytometry

Nuclei were prepared according to the Vindelov technique (25). Briefly, cells were harvested by gentle scraping, pelleted by low speed centrifugation and resuspended in 70 μl of citrate buffer (250 mM sucrose, 40 mM trisodium citrate, 5% DMSO, pH 7.6). Then cells were treated with 350 μl of trypsin (30 μg/ml; Sigma) for 10 min at room temperature followed by treatment with 300 μl of trypsin inhibitor (0.5 mg/ml; Sigma) and RNase A (0.1 mg/ml). Nuclei were stained with 300 μl of ice-cold staining solution (0.4 mg/ml propidium iodide, 1.16 mg/ml spermine) and analyzed by flow cytometry. All solutions were prepared in a stock solution containing 3.4 mM trisodium citrate, 0.1% (v/v) Nonidet P-40, 1.5 mM spermine, 0.5 mM Tris base, pH 7.6.

Enzyme-linked immunosorbent assay (ELISA)

Measurement of $p21^{WAF1/Cip1}$ antigen in the nuclear fraction was performed using ELISA according to the manufacturer's instructions (Calbiochem, Meudon, France).

Invasion assay on a Matrigel-coated membrane in a Transwell

After treatment cells were detached with non-enzymatic cell dissociation solution, washed twice in PBS and resuspended in RPMI 1640 with 0.2 mg/ml bovine serum albumin (BSA) (Sigma). Cells (5×10^4) were seeded in the upper chamber of a Transwell insert (12 μM diameters pores; Dutscher) coated with Matrigel (diluted 1:100) (Becton Dickinson, Franklin Lakes, NJ). The lower chamber was filled with 1 ml of RPMI 1640 together with 2 mg/ml BSA and basic fibroblast growth factor (20 ng/ml; R&D Systems, Abingdon, UK) to induce chemotaxis. After 18 h incubation the non-migrated cells in the upper chamber were gently scraped away and adherent cells present on the lower surface of the insert were stained with May–Grünewald–Giemsa.

Confocal microscopy analysis of Ras and RhoA on MDA-MB-231 cells

MDA-MB-231 cells were cultured in 4-well Glass Lab-Tek chamber slides (Nunc, Roskilde, Denmark). After washing in PBS cells were fixed for 15 min at room temperature with 3.5% paraformaldehyde and permeabilized with 1% Triton X-100 for 5 min. Ras and RhoA were detected using primary monoclonal antibodies (from Transduction Laboratories, Lexington, KY and Santa Cruz Biotechnology, Santa Cruz, CA, respectively) at a concentration of 2 μg/ml (1 h, room temperature). After washing, cells were incubated with a secondary FITC-conjugated anti-mouse IgG antibody (1:200; Dako) for 40 min at room temperature. Actin filaments were visualized by TR/TC labelled phalloidin, computer-assisted image analysis of immunofluorescence was performed using a confocal scanning laser microscope (Leica TCS; excitation wavelength 488 nm, emission 525 nm for FITC and 580 nm for TRITC).

Electrophoretic mobility shift assay (EMSA)

Nuclear proteins were prepared as described previously (26). The protein concentration was determined according to the method of Bradford (27) using the Bio-Rad protein assay (Hercules, CA). The DNA–protein reaction was performed as previously described (26) using 10 μg nuclear extracts and a ^{32}P 5′-end-labeled oligonucleotide coding for the tandem κB sequence from the human immunodeficiency virus long terminal repeat enhancer (28,29). The resulting protein–oligonucleotide complexes were resolved by 6% PAGE and visualized by autoradiography. For supershift assay nuclear extracts were preincubated for 30 min on ice with antibodies against RelA (p65), p50, RelB or c-Rel (polyclonal antibodies from Santa Cruz Biotechnology) before the binding reaction.

Cellular localization of NFκB by immunofluorescence

Immunofluorescence was performed on MDA-MB-231 cells cultured in 4-well Lab-Tek chamber slides. After incubation, cells were washed in PBS fixed with 3.5% paraformaldehyde for 15 min and permeabilized with 1% Triton X-100. Fixed cells were incubated for 1 h at room temperature in PBS with 1% BSA (Sigma) to avoid non-specific binding. Detection of NFκB was carried out by incubating cells with a polyclonal primary antibody against RelA (1 μg/ml; Santa Cruz Biotechnology) for 1 h at room temperature. After washing, cells were incubated with a secondary FITC-conjugated anti-rabbit IgG antibody (Dako, Trappes, France) for 40 min at room temperature. A

control with a non-relevant antibody of the same isotype was performed to evaluate non-specific fluorescence. Green fluorescence was visualized with a fluorescence microscope (Leica Leitz DMRB).

Western blot analysis

Cytoplasmic extracts from breast cancer cell lines were prepared by hypotonic disruption of cells (5 mM HEPES, 1.5 mM $MgCl_2$, 10 mM KCl, 0.5 mM dithiothreitol, 0.1 mM phenylmethylsulfonyl fluoride and 0.1 mM aprotinin). Equal amounts of protein extracts (20 µg) were subjected to PAGE (10% for IκBα and 12.5% for $p21^{Waf1/Cip1}$) under denaturing conditions (SDS–PAGE). Proteins were electrotransferred onto polyvinylidene difluoride membranes (Amersham, Saclay, France) using a semi-dry system (Schleicher & Schuell, Dassel, Germany). The efficiency of electrotransfer was assessed by Ponceau Red (Sigma) staining. Binding of the primary antibody against IκBα (1:150 MAD10B) (30) and $p21^{Waf1/Cip1}$ (1:500; Transduction Laboratories) was detected with the enhanced chemiluminescence visualization system (ECL, Amersham) using horseradish peroxidase-coupled anti-mouse antibody (1:10 000; Dako). Autoradiography was carried out for 1–10 min.

Flow cytometry analysis

Surface expression of TF was analyzed by direct immunofluorescence using flow cytometry. Briefly, adherent cells were detached with non-enzymatic cell dissociation solution (Sigma) and washed twice in cold PBS. Approximately 10^6 cells were incubated for 15 min at 4°C with 10 µl of FITC-conjugated anti-TF antibody (50 µg/ml; American Diagnostic, Greenwich, CT). After two washes in PBS the cell suspension was analyzed in a flow cytometer (EPICS XL-MCL; Coulter, USA).

u-PA associated with the cell surface was analyzed by indirect fluorescence. Cells were first incubated with 10 µl of a primary anti-u-PA antibody (0.5 mg/ml; American Diagnostic). After 15 min at 4°C the cells were washed twice and incubated with 100 µl of a 1:100 dilution of a FITC-conjugated anti-mouse IgG1 (1 mg/ml; Immunotech) and analyzed by flow cytometry after two additional washes.

Data are expressed as the specific mean channel fluorescence intensity, which was calculated for each sample by subtracting the background channel fluorescence intensity produced by the negative control (irrelevant antibody) from the channel fluorescence intensity value generated by the specific antibody. Photomultiplier voltage remained the same for all measurements in all experiments.

Total RNA extraction and RT–PCR

Briefly, after treatment cells were detached with the non-enzymatic cell dissociation solution and washed twice in PBS. Total RNA extraction was performed using the SV Total RNA Isolation System (Promega) according to the manufacturer's instructions.

Primers were chosen using a biomolecular sequences database (GenBank) and oligonucleotides were synthesized by Genset (Paris, France). The sequences were as follows: $p21^{Waf1/Cip1}$ sense primer, 5′-CGGAGCTGG-GCGCGGATTCG-3′ (nt 27–46 in exon 1), antisense primer, 5′-GGAAGCGC-GAGGGCCTCAAA-3′ (nt 599–619 in exon 2); β-actin sense primer, 5′-ATCTGGCACCACACCTTCTACAATGAGCTGCG-3′ (nt 253–284 in exon 3), antisense primer, 5′-CGTCATACTCCTGCTTGCTGATCCACATC-TGC-3′ (nt 1049–1080 in exon 6).

RT–PCR was performed using the Access RT–PCR System (Promega) and was conducted in a total volume of 50 µl containing 10 µl of AMV/*Tfl* 5× reaction buffer, 0.2 mM dNTP, 1 µM sense and antisense primers, 1 mM $MgSO_4$, 1 U AMV reverse transcriptase, 1 U *Tfl* DNA polymerase and 5 µl of total RNA, denatured beforehand for 2 min at 94°C. Reverse transcription was performed at 48°C for 45 min. The reaction products were then subjected to 30 cycles of PCR. The amplification cycle consisted of 30 s at 94°C for denaturation, 30 s at 65 and 60°C ($p21^{Waf1/Cip1}$ and β-actin, respectively) for primer annealing and 30 s at 68°C for extension. Finally, a step extension at 68°C for 7 min improved the quality of the final product by extending the truncated product to full length. An aliquot of 10 µl of PCR products and a standard DNA ladder were size fractionated through a 2% agarose gel stained with ethidium bromide (1%). The predicted sizes for $p21^{Waf1/Cip1}$ and β-actin PCR products were 592 and 838 bp, respectively.

SDS–PAGE zymography and TIMP-1 secretion

MDA-MB-231 cells were incubated for 18 and 36 h in serum-free medium and increasing concentrations of cerivastatin. Conditioned medium was collected, centrifuged and the supernatants frozen until analysis. Electrophoresis was performed on samples of 10 µl of conditioned medium/lane on 7.5% polyacrylamide gels containing 10% SDS and gelatin (1 mg/ml) under non-reducing conditions. After electrophoresis SDS was removed from the gels by washing for 1 h in 2.5% Triton X-100 at room temperature. Gelatinase activity was revealed overnight at 37°C in a buffer containing 50 mM Tris–HCl and 5 mM $CaCl_2$. The gels were stained with 0.25% Coomassie Blue R250 (Sigma) and gelatinolytic activity was observed as clear bands against the blue background of stained gelatin. TIMP-1 secretion was also measured in the conditioned medium of MDA-MB-231 cells using an ELISA kit (Calbiochem) according to the manufacturer's instructions.

Statistical analysis

Significance was determined by Student's *t*-test using Instat software (Sigma). All results are expressed as means ± SEM.

Results

Inhibition of MDA-MB-231 cell proliferation by cerivastatin

Cerivastatin induced a dose-dependent decrease in cell proliferation of MDA-MB-231 cells (up to 40% inhibition at 25 ng/ml) (Figure 1). A cytotoxic effect was observed at higher concentrations (50 ng/ml), as confirmed by incorporation of Trypan blue, which was accompanied by cell detachment from the surface. The inhibitory effect of cerivastatin on MDA-MB-231 cell proliferation was fully reversible by co-incubation with 100 µM MVA or 10 µM GGPP, but not 10 µM FPP.

After 2 days morphological changes in cells treated with 25 ng/ml cerivastatin were observed: they became larger and rounder (Figure 2). These cell shape changes were prevented by addition of 10 µM GGPP with cerivastatin, while 10 µM FPP was without effect (data not shown).

In contrast, cerivastatin treatment did not significantly modify MCF-7 cell proliferation, but at 50 ng/ml slight Trypan blue incorporation was noted (Figure 1).

Cerivastatin does not induce apoptosis

To determine whether cerivastatin induced apoptosis of breast cancer cells we performed three assays.

Firstly, cerivastatin treatment did not induce annexin V binding to the cell membrane, an early marker of apoptotic cells (Table I). Moreover, propidium iodide incorporation was not observed, confirming the absence of cell membrane permeability (Table I).

Secondly, as shown by gel migration of genomic DNA, cerivastatin did not induce chromatin cleavage to oligonucleosomal fragments, an indicator of caspase-3 activity (Figure 3, lane 2). In contrast, TNF-α, previously described as inducing apoptosis of MDA-MB-231 cells, induced the characteristic apoptotic DNA ladder (Figure 3, lane 3).

Thirdly, when examining propidium iodide stained DNA by flow cytometry the sub-diploid population (apoptotic cells) was not increased (~2% of total cell population) by cerivastatin, whereas TNF-α-induced apoptosis was clearly evident as an increase in the pre-G_1 peak (24.5% of cells) (Table II).

Cerivastatin induces a cell cycle block in G_1/S phase

Flow cytometry analysis showed that cerivastatin induced an arrest of the cell cycle in G_1/S phase (67.1% in cerivastatin-treated cells versus 58.9% in controls) after 36 h treatment. This arrest was not observed for a shorter incubation time (18 h). The proteasome inhibitor MG-132, known to induce cell cycle blockade in G_2/M, was used as a control. The results are given in Table II.

Cerivastatin increases $p21^{Waf1/Cip1}$ mRNA and protein expression

We studied whether cerivastatin induces the cyclin-dependent kinase inhibitor (cdki) $p21^{Waf1/Cip1}$, mainly involved in the G_1/S transition, in MDA-MB-231 cells. Western blot analysis (Figure 4.2, lane 2) and ELISA (Figure 4.3) of nuclear extracts showed that cerivastatin induced a marked increase in the level of $p21^{Waf1/Cip1}$.

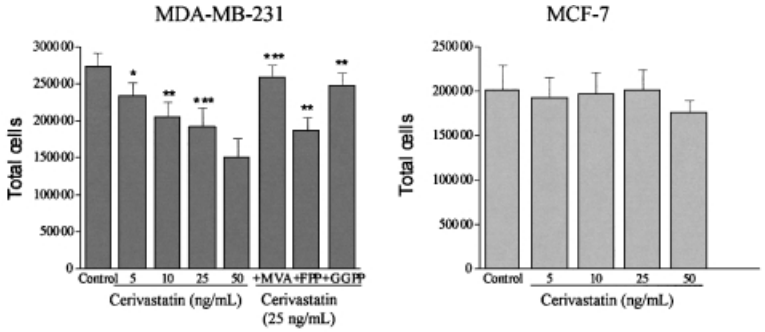

Fig. 1. Dose-dependent inhibition of MDA-MB-231 cell proliferation by cerivastatin. Cells (5×10^5) were seeded and after 3 or 5 days culture (MDA-MB-231 and MCF-7 cells, respectively) with a minimal concentration of fetal calf serum (2%) to ensure viability were counted in a particle counter. Total cells = adherent + supernatant cells. Results are means ± SEM of three independent experiments (*$P < 0.05$, **$P < 0.01$, ***$P < 0.001$).

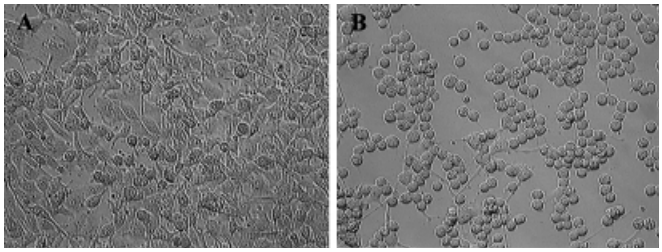

Fig. 2. Morphological changes in MDA-MB 231 cells induced by cerivastatin. Cells were cultured for 2 days in the absence (**A**) or presence (**B**) of cerivastatin (25 ng/ml) and examined by phase contrast microscopy (×40). Note the cell rounding and swelling.

Table I. Absence of apoptosis in MDA-MB-231 cells treated with cerivastatin

Stain	Control	Cerivastin (ng/ml)			
		5	10	25	50
Annexin V	8.6 ± 3.6	9.3 ± 1.5	8.2 ± 2.9	10.6 ± 1.3	9.1 ± 1.8
Propidium iodide	5.6 ± 1.6	5.1 ± 0.2	3.9 ± 0.9	3.4 ± 0.7	3.3 ± 0.6

MDA-MB-231 cells were treated for 36 h with cerivastatin. Annexin V and propidium iodide incorporation by MDA-MB-231 cells were determined by flow cytometry, as described in Materials and methods. Results are the means ± SEM of three independent experiments and are expressed as the percentage of positive fluorescent cells.

As ubiquitin-mediated proteolysis is involved in the turnover of various cell cycle regulatory proteins, including cdki, we also studied the effect of MG-132, a proteasome inhibitor, on $p21^{Waf1/Cip1}$ mRNA and protein levels. We observed that MG-132 increased $p21^{Waf1/Cip1}$ protein levels (Figure 4.2, lane 3, and Figure 4.3), but this effect was less intense than that of cerivastatin. The p21 transcript was increased in MDA-MB-231 cells after cerivastatin treatment, while MG-132 had no effect on mRNA expression, suggesting a proteasome-independent effect (Figure 4.1, lanes 2 and 3, respectively). The MCF-7 cell line, known to exhibit high basal levels of $p21^{Waf1/Cip1}$, was used as a control (Figure 4.1 and 4.2, lanes 4, and Figure 4.3).

In order to investigate whether RhoA or Ras inactivation accounts for the induction of $p21^{Waf1/Cip1}$ we analyzed the effects of MVA, FPP and GGPP (Figure 4.3). When MDA-MB-231 cells were treated with cerivastatin together with 100 μM MVA, 10 μM GGPP or 10 μM FPP only MVA and GGPP reversed the stimulating effect of cerivastatin on $p21^{Waf1/Cip1}$ expression.

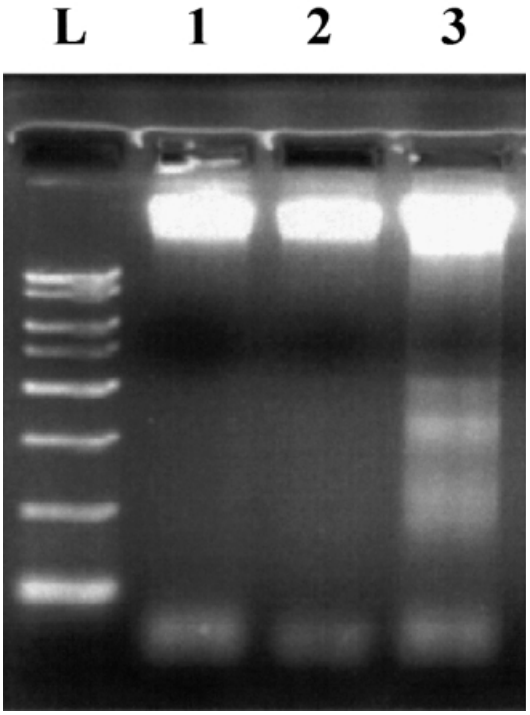

Fig. 3. Absence of apoptosis in MDA-MB-231 cells treated with cerivastatin. MDA-MB-231 cells were treated for 36 h with 25 ng/ml cerivastatin (lane 2) or 50 ng/ml TNF-α (lane 3). Control (lane 1) genomic DNA was collected and separated by agarose gel electrophoresis (2%). Note the typical DNA fragmentation induced by TNF-α treatment. L, ladder.

Cerivastatin inhibits invasion of MDA-MB-231 cells through Matrigel

Under laboratory conditions MDA-MB-231 cells migrated through Matrigel, whereas MCF-7 cells did not. Cerivastatin dose dependently inhibited cell invasion through Matrigel, with a plateau at 25 ng/ml (54 ± 5.1% inhibition of migration, $P < 0.01$) (Figure 5.1 and 5.2). This inhibitory effect of cerivastatin was rescued by MVA and GGPP, but not FPP (Figure 5.1).

Cerivastatin delocalizes RhoA and Ras from the membrane to the cytosol and induces morphological changes

The membrane localization of RhoA protein in untreated cells (Figure 6A) was significantly decreased by an 18 h treatment with cerivastatin (Figure 6B). When cells were treated with both cerivastatin and GGPP (Figure 6E) the effect of cerivastatin was reversed and RhoA was associated with the cell membrane. In contrast, FPP did not prevent the effect of cerivastatin

Table II. Arrest in G_0/G_1 phase of the cell cycle in cerivastatin-treated MDA-MB-231 cells

	Cells in each phase of the cell cycle (%)			
	sub-G_1	G_0/G_1	S	G_2/M
(A) Control (18 h)	1.9	58.9	27.1	12.1
(B) Cerivastatin (18 h)	1.8	59.9	25.2	13.1
(C) MG-132 (18 h)	1.8	44.5	26.3	**27.4**
(D) Control (36 h)	2.1	57.0	30.0	10.9
(E) Cerivastatin (36 h)	2.0	**67.1**	24.1	6.8
(F) TNF-α (36 h)	**24.5**	47.1	22.7	5.7

Cell cycle distribution was studied by flow cytometry according to Vindelov's technique. MDA-MB-231 cells were treated for 18 (B) or 36 h (E) with cerivastatin (25 ng/ml). MG-132 (10 μM) was used as a positive control for G_2/M arrest of the cell cycle (C) and TNF-α (50 ng/ml) was used as a positive control for apoptosis (a pre-G_1 peak is characteristic of apoptotic cells) (F). Results are means (representative of five independent experiments). Bold numbers indicate the principal modifications induced by the treatment.

(Figure 6D). Interestingly, cell membrane-associated RhoA was mainly distributed in patches, suggesting that activated RhoA was associated with caveolae-enriched membrane domains, as previously reported (31). As RhoA is involved in the regulation and assembly of contractile actin filaments (stress fibers) and in associated focal adhesion complexes, we studied the effect of cerivastatin on actin filaments in MDA-MB-231 cells. Various stress fibers and dense focal adhesions were detected in untreated cells stained with fluorescent phalloidin (Figure 6F). After 18 h cerivastatin caused a dramatic change in cell shape (Figure 6G); cells became rounder with only a few organized actin filaments and loss of focal adhesion points, while in untreated cells a dense and mesh-like network was still observed (Figure 6F). Disorganization of actin fibers was complete after 36 h (Figure 6H). The action of cerivastatin on actin disorganization was prevented by GGPP, but not by FPP (Figure 6J and I, respectively). A membrane location of Ras was observed by confocal microscopy in untreated MDA-MB-231 cells (Figure 6K). After 18 h treatment with cerivastatin we still observed a membrane location of Ras (Figure 6L). Delocalization of Ras to the perinuclear region was only observed after 36 h treatment with cerivastatin (Figure 6M). However, cerivastatin-induced translocation of Ras from the cell surface to the cytoplasm was much weaker than that observed for RhoA. Furthermore, we did not observe any reversion of this translocation by GGPP and FPP (Figure 6O and N, respectively). This could indicate that constitutive Ras activation of MDA-MB-231 cells is poorly regulated by isoprenoid compounds.

Cerivastatin decreases NFκB constitutive activity in MDA-MB-231 cells and concomitantly increases IκB

Activation of NFκB factors was determined by the capacity of nuclear proteins to specifically bind κB oligonucleotides (EMSA) and by the subcellular localization of the RelA subunit (*in situ* immunofluorescence).

First, EMSAs were performed with nuclear extracts from the two breast cancer cell lines. These results are shown in Figure 7.1 (only the retarded oligonucleotide is shown). Consistent with previous reports (20), constitutive activation of NFκB in MDA-MB-231 cells was evident as a high level of NFκB–DNA binding (lane 1). On the other hand, the results of the EMSA indicate that MCF-7 cells show no constitutive

Figure 4-1.

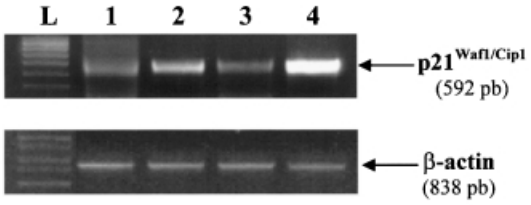

Figure 4-2.

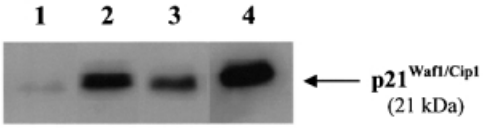

Figure 4-3.

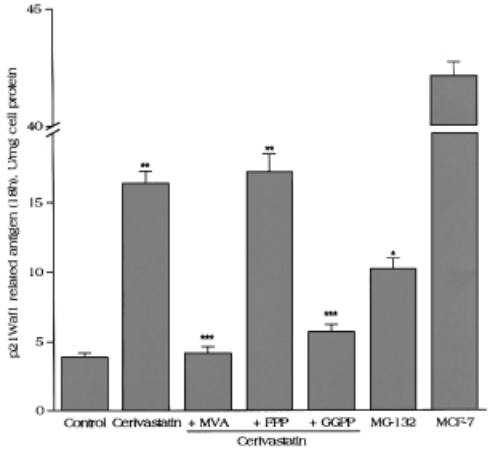

Fig. 4. Effect of cerivastatin on $p21^{Waf1/Cip1}$ mRNA expression and nuclear protein level in MDA-MB-231 cells. Comparison with the effect induced by MG-132. (**1**) Analysis of $p21^{Waf1/Cip1}$ mRNA expression by RT–PCR. MDA-MB-231 cells were incubated for 12 h with 25 ng/ml cerivastatin (lane 2) or 10 μM MG-132 (lane 3) and compared with untreated cells (lane 1). MCF-7 cells were used as a positive control since they express elevated levels of $p21^{Waf1/Cip1}$. The sizes of PCR products for $p21^{Waf1/Cip1}$ and β-actin were 592 and 838 bp, respectively. L, ladder. (**2**) Analysis of $p21^{Waf1/Cip1}$ expression by western blot. Analysis of nuclear extracts of cerivastatin-treated MDA-MB-231 cells using a monoclonal anti-$p21^{Waf1/Cip1}$ antibody. Blots were developed with the enhanced chemiluminescence reagent (ECL). Lane 1, control (18 h); lane 2, 25 ng/ml cerivastatin (18 h); lane 3, 10 μM MG-132 (18 h); lane 4, untreated MCF-7 cells. (**3**) Quantification of $p21^{Waf1/Cip1}$ protein level by ELISA. Results are the means ± SEM of six independent experiments (*$P < 0.05$, **$P < 0.01$, ***$P < 0.001$).

activation of NFκB (data not shown). Specific binding of NFκB to DNA was abrogated by an excess of unlabeled probe containing the NFκB motif (data not shown). In untreated MDA-MB-231 cells the DNA-binding complex was constituted of NFκB heterodimer (RelA/p50), as demonstrated by supershifting experiments (lanes 8–11). Cerivastatin-treated MDA-MB-231 cells showed a time-dependent and significant decrease in NFκB DNA-binding activity (lanes 2–4). This deactivation of NFκB began 18 h after incubation with cerivastatin and was complete at 36 h. As a control we used a proteasome inhibitor, MG-132, which prevents IκB degradation. As expected, after a 4 h treatment NFκB DNA-binding activity was abolished (lane 5). Nevertheless, we noticed a transient effect of MG-132, because after 18 h NFκB activity returned to its original level (lane 6).

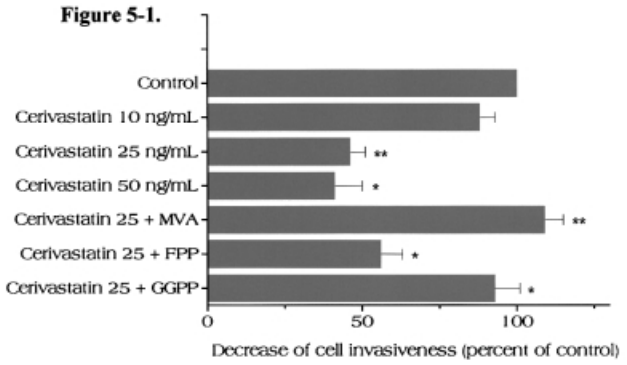

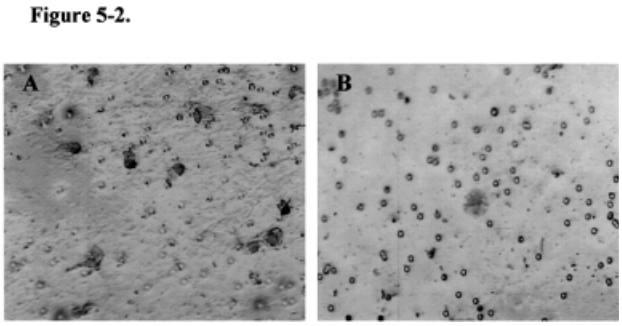

Fig. 5. Inhibition of MDA-MB-231 cell invasion by cerivastatin. (**1**) Effect of increasing concentrations of cerivastatin on MDA-MB-231 invasiveness through Matrigel. MDA-MB-231 cells were incubated with cerivastatin for 18 h and then harvested in the upper Transwell chamber coated with Matrigel, as described in Materials and methods. Then the cells in the upper part of the invasion chamber were gently scraped away and cells which had crossed the filter were counted by light microscopy after May–Grünewald–Giemsa staining. Results are means ± SEM of five independent experiments (*$P < 0.05$, **$P < 0.01$). (**2**) Photographs of MDA-MB-231 cells after invasion through Matrigel. Note the morphological aspect of untreated (**A**) and cerivastatin-treated (**B**) MDA-MB-231 cells (×40).

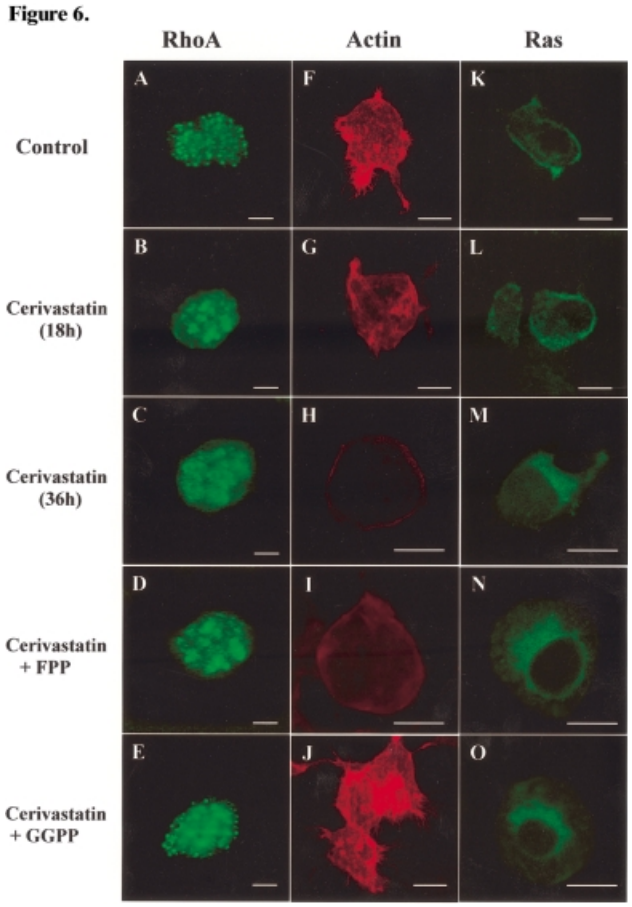

Fig. 6. Modification of the localization of RhoA and Ras and reorganization of the actin cytoskeleton in MDA-MB-231 cells treated with cerivastatin. The localization of RhoA and Ras and the organization of the actin cytoskeleton were analyzed by confocal microscopy of untreated cells (**A**, **K** and **F**, respectively) or after 18 h (**B**, **L** and **G**, respectively) or 36 h (**C**, **M** and **H**, respectively) cerivastatin treatment (25 ng/ml). Note the presence of focal adhesion attachment sites in untreated cells (F). Treatment with cerivastatin induced progressive morphological changes in cells associated with translocation of RhoA (18 h) and Ras (36 h) from the cell membrane to the cytoplasm and disorganization of the actin stress fibers. Addition of GGPP resulted in nearly complete fixation of RhoA at the cell membrane (**E**) and in reorganization of the cytoskeleton (**J**), while FPP had no effect (**D** and **I**, respectively). In contrast, addition of GGPP and FPP with cerivastatin did not prevent the effects of cerivastatin on Ras delocalization (**O** and **N**, respectively). Scale bar 10 μm.

Secondly, immunofluorescence staining of the RelA subunit in MDA-MB-231 cells (Figure 7.2) showed a mainly nuclear localization, with significantly less cytoplasmic fluorescence (Figure 7.2A) (nuclei were identified by incorporation of propidium iodide; Figure 7.2A' and D'). In contrast, in MCF-7 cells, which do not express constitutive nuclear NFκB, the RelA subunit was primarily located in the cytoplasm (data not shown). After 18 h incubation with cerivastatin (Figure 7.2B) large amounts of the RelA subunit were found in the cytoplasm, although some p65 still remained in the nucleus. In addition, the inhibitory effect of NFκB activity induced by cerivastatin was prevented by co-incubation with GGPP, but not FPP (Figure 7.2D and C, respectively). This indicates that inhibition of NFκB by cerivastatin is related to RhoA inhibition.

Finally, simultaneous with the decrease in NFκB activity in cerivastatin-treated cells we observed a time-dependent increase in IκB protein in the cytoplasmic extract by western blot (Figure 7.3).

Effect of cerivastatin on TF and u-PA expression in MDA-MB-231 cells

As NFκB is clearly involved in expression of TF and u-PA, we analyzed both TF and u-PA by flow cytometry. After 18 h incubation with cerivastatin we noted a dose-dependent decrease in TF expression on the MDA-MB-231 cell surface (63% decrease at 25 ng/ml) (Table III). This decrease was associated with a decrease in TF mRNA (data not shown). In contrast, no significant modification of u-PA expression was detected after 18 h incubation with cerivastatin, a significant decrease occurring only after a 2 day treatment (59% decrease at 25 ng/ml) (Table III). Moreover, the decrease in u-PA expressed on the cell surface was associated with a decrease in u-PA activity (data not shown). This late decrease in u-PA expression correlated with a decrease in mRNA (data not shown). In comparison, the decrease in u-PA induced by an inhibitor of NFκB, MG-132, was more evident from 18 h, while TF expression was not modified (Table III).

In MCF-7 cells TF and u-PA expression was not modified by cerivastatin at 5–50 ng/ml nor by MG-132, as expected, since there was no constitutive activation of NFκB in these cells (data not shown).

Effect of cerivastatin on MMP-9 secretion by MDA-MB-231 cells

MDA-MB-231 cells were incubated for 18 and 36 h with increasing concentrations of cerivastatin. The conditioned

Figure 7-1.

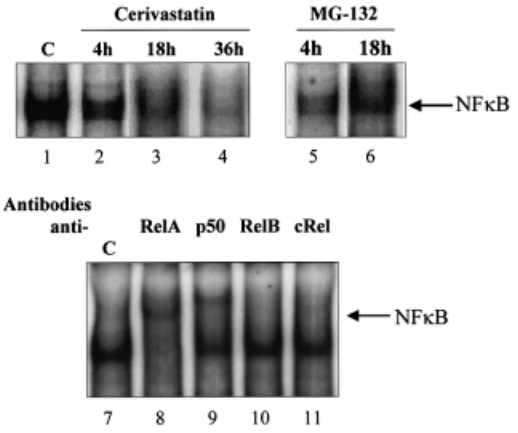

Figure 7-2.

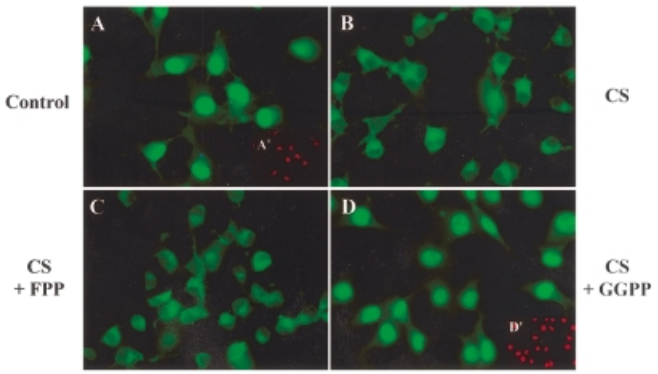

Figure 7-3.

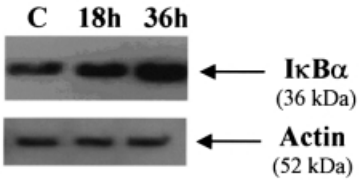

Fig. 7. Cerivastatin decreases NFκB activity in MDA-MB-231 cells. (**1**) NFκB DNA-binding activity by EMSA and supershift assay. Nuclear cell extracts (10 μg) were incubated with double-stranded oligonucleotide containing a NFκB binding site and subjected to EMSA, as indicated in Material and methods. The results indicate constitutive DNA-binding activity in MDA-MB 231 cells (lane 1). Inhibition of NFκB binding activity by cerivastatin (lanes 2–4) is time dependent in MDA-MB-231 cells. MG-132 (lane 5) was used as a positive control. Note that this inhibiting effect was delayed by cerivastatin in comparison and transient with MG-132 (lane 6). The identity of the complex was determined by supershifting the protein–oligonucleotide complex with RelA- (lane 8) and p50-specific (lane 9) antisera. RelB (lane 10) and c-Rel (lane 11) antibodies had no effect on complex migration. The arrow indicates the position of the supershifted bands. (**2**) Cell localization of the NFκB p65 subunit detected by *in situ* immunofluorescence. In untreated cells (**A**) p65 subunit localization was almost entirely nuclear, while treatment with cerivastatin (**B**) induced translocation of the RelA (p65) subunit from the nucleus to the cytoplasm. Repletion of cerivastatin-treated cells with GGPP fully reversed the cerivastatin inhibition of NFκB activity (**D**). In contrast, FPP was without effect (**C**). Nuclei were identified by incorporation of propidium iodide (**A′** and **D′**). (A) and (D), ×100; (B) and (C), ×40. (**3**) Analysis of IκBα expression by western blot. MDA-MB-231 cells were treated for 18 (lane 2) or 36 h (lane 3) with 25 ng/ml cerivastatin. Cytoplasmic extracts were subjected to SDS–PAGE and western blot analysis using an anti-IκBα antibody. Lane 1, control. Blots were rehybridized with β-actin to control protein loading.

Table III. Effect of cerivastatin and MG-132 on TF and u-PA expression in MDA-MB-231 cells

	Cerivastatin (ng/ml) 18 h				Cerivastatin (ng/ml) 36 h				MG-132 (μM) 18 h			
	5	10	25	50	5	10	25	50	5	10	25	50
TF	71.9 ± 3.1[a]	49.1 ± 5.6[a]	37.5 ± 1.4[b]	39.2 ± 5.9	nd	nd	nd	nd	110.4 ± 3.6	117.4 ± 2.9	119.5 ± 4.4	107.9 ± 3.2
u-PA	97.5 ± 0.9	93.2 ± 3.8	86.5 ± 5.9	90.1 ± 2.7	59.6 ± 4.1[a]	47.7 ± 3.2[b]	41.1 ± 5.4[a]	39.2 ± 2.6[a]	89.4 ± 5.2	60.8 ± 3.2[c]	57.4 ± 3.7[b]	54.8 ± 4.4[c]

Confluent monolayers of MDA-MB-231 cells were incubated for 18 or 36 h with cerivastatin and for 18 h with MG-132 at the indicated concentrations. Results are means ± SEM of five independent experiments and expressed as a percentage of mean fluorescence intensity as compared with the mean fluorescence intensity of the control. nd, not determined.

[a] $P < 0.05$.
[b] $P < 0.01$.
[c] $P < 0.001$.

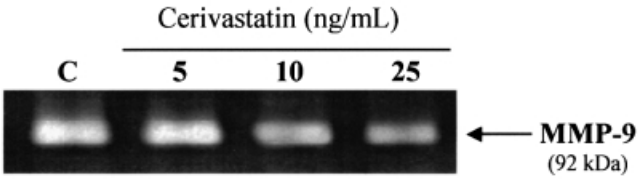

Fig. 8. Representative gelatin zymography gel showing the effect of cerivastatin on MMP-9 secretion by MDA-MB-231 cells. MDA-MB-231 cells were incubated for 36 h at the indicated concentrations of cerivastatin. Conditioned medium was collected and MMP-9 (92 000 kDa type IV collagenase) secretion assessed by gelatin zymography. Molecular weights were determined using pre-stained standards. This experiment is representative of five distinct experiments.

Table IV. Effect of cerivastatin on TIMP-1 secretion by MDA-MB-231 cells

	Control	Cerivastatin (ng/ml)		
		10	25	50
TIMP-1 secretion (% of control)	100	87.2 ± 4.3	104.1 ± 8.3	97.6 ± 5.5

MDA-MB-231 cells were incubated in serum-free medium at the indicated concentrations of cerivastatin for 36 h. TIMP-1 secretion was determined by ELISA in the conditioned medium of these cells, as described in Materials and methods. Results are the means ± SEM of three distinct experiments and are expressed as a percentage of the control untreated MDA-MB-231 cells.

medium was then collected and analyzed by direct gelatin zymography. MDA-MB-231 cells constitutively secreted high levels of M_r 92 000 MMP-9 (Figure 8). No significant modification of MMP-9 secretion was observed after 18 h incubation with cerivastatin (data not shown), whereas cerivastatin dose-dependently reduced these levels in MDA-MB-231 cells only after 36 h treatment (Figure 8). The decrease in MMP-9 secretion was not due to a toxic effect of cerivastatin on MDA-MB-231 cells, which would decrease the secretion of all protein, since, for example, secretion of TIMP-1, an inhibitor of MMP-9, was unaffected by cerivastatin treatment (Table IV).

Discussion

Despite an initial favorable response to chemotherapy for breast cancer, a high percentage of patients experience relapse and die of their disease (32). Clearly the association of chemotherapy with new therapeutical approaches should be considered. In a recent double blind study it was shown that the incidence of cancer was reduced in a group of patients treated with a HMG-CoA reductase inhibitor in comparison with a placebo group (3). However, in this series all tumors were taken into consideration, without indicating the type of cancer. In our study we evaluated the benefit of the HMG-CoA reductase inhibitor cerivastatin on the MDA-MB-231 breast cancer cell line, characterized by constitutive activation of Ras (6), overexpression of activated Rho (7) and activation of NFκB (14). The effects of cerivastatin were compared with those on MCF-7 cells, a poorly invasive breast cancer cell line.

At low concentrations we found that cerivastatin induced a dose-dependent decrease in MDA-MB-231 cell proliferation, with up to 40% inhibition at 25 ng/ml. This inhibitory effect was not due to apoptosis as cerivastatin did not induce any DNA fragmentation, annexin V binding to the cell membrane or a pre-G_1 peak increment. At concentrations up to 25 ng/ml cerivastatin showed no cytotoxic effects, but higher concentrations (50 ng/ml) clearly affected cell viability. Cell toxicity was preceded by cell rounding and was characterized by detachment of the cells from the culture flask, which could have been responsible for the loss of cell survival signals. Interestingly, cerivastatin did not modify cell proliferation (up to 25 ng/ml) of poorly invasive MCF-7 cells.

In addition, we observed that cerivastatin also displayed a potent anti-invasive effect on MDA-MB-231 cells, revealed as a significant decrease in MDA-MB-231 cell invasion through Matrigel (54% decrease). This decrease in cell invasiveness was observed after 18 h incubation with cerivastatin. This effect of cerivastatin was not tested on MCF-7 cells because these cells are not invasive.

We suggest that cerivastatin may inhibit both proliferation and invasiveness of highly invasive cancer cells by its ability to inactivate Ras and RhoA for two reasons. Firstly, cerivastatin prevents the synthesis of isoprenoid derivatives such as FPP and GGPP, responsible for the targeting of Ras and RhoA, respectively, to the cell membrane, a step required for their cell signaling (4). Secondly, Ras and RhoA are known to regulate signal transduction involved in a variety of cellular processes, including cell morphology (33), cell motility (9), cell proliferation (34,35) and tumor progression (36–38).

The inhibitory effect of cerivastatin on both proliferation and invasivness of MDA-MB-231 cells was clearly related to inhibition of the biosynthesis of prenylated derivatives because it was shown to be reversed by MVA, the precursor of FPP and GGPP.

In order to assess which of these two pathways, Ras prenylation (FPP) or RhoA prenylation (GGPP), was responsible for the anti-proliferative and anti-invasive effects of cerivastatin, we investigated the reversibility of cerivastatin activity by FPP and by GGPP.

As regards the anti-proliferative effect of cerivastatin on MDA-MB-231 cells, we observed that this inhibitory effect was reversed only on addition of GGPP. Accordingly, a possible anti-proliferative effect related to Ras pathway inhibition was excluded since it was not reversed by FPP. Therefore, inhibition of MDA-MB-231 cell proliferation by cerivastatin could be related to inhibition of the Rho-dependent pathway rather than inhibition of the Ras-dependent MAPK pathway. Moreover, this anti-proliferative effect was related to arrest of the cell cycle in G_1/S phase. As previously reported for lovastatin (39), this inhibition of cell proliferation is associated with an increase in the amount of $p21^{Waf1/Cip1}$, a cdki predominantly involved in the G_1/S transition. In our study we demonstrate that this increase in $p21^{Waf1/Cip1}$ is caused by increased synthesis and not by a decrease in proteasome-induced degradation, as observed with an inhibitor of NFκB, MG-132 (40). Indeed, cerivastatin induced an increase in $p21^{Waf1/Cip1}$ transcript, while MG-132 did not. Recently it was shown that geranylgeranylation of RhoA is required to suppress $p21^{Waf1/Cip1}$ transcription, promoting cell progression and cell proliferation (8). Therefore, these results strengthen the hypothesis that inhibition of MDA-MB-231 cell proliferation by cerivastatin is due to inhibition of RhoA prenylation. This is in agreement with the delocalization of RhoA from the cell membrane to the cytosol in MDA-MB-231 cells and its reversion by GGPP, as observed by confocal microscopy (Figure 6).

We have also studied the mechanism of cerivastatin action with regard to the anti-invasive effect of cerivastatin on MDA-MB-231 cells.

Two complementary mechanisms could contribute to the inhibitory effect induced by cerivastatin on MDA-MB-231 invasiveness and migration. The first mechanism by which cerivastatin confers its anti-invasive effect could be related to NFκB inhibition. RhoA and Ras stimulate NFκB-dependent transcription (12,13). NFκB, which is constitutively activated in MDA-MB-231 cells (14; present paper), was deactivated by cerivastatin treatment, as shown both by delocalization of the RelA (p65) subunit from the nucleus to the cytoplasm and by a decrease in DNA binding by gel shift assay. This inhibitory effect of cerivastatin on NFκB activity was observed from 18 h incubation and was rescued by addition of GGPP, but not by FPP. However, we cannot rule out that inhibition of NFκB translocation is related to an increase in IκB, as shown in Figure 7.3.

Thus, our results suggest that the inhibitory effect of cerivastatin on MDA-MB-231 cell invasiveness is mostly due to RhoA inhibition rather than Ras inhibition. This is in agreement with the translocation of Ras from the cell membrane to the cytoplasm induced by cerivastatin, which was only partial and required a longer time than the observed effects on proliferation and invasiveness; inhibition of translocation requires at least 36 h while the inhibitory effect on cell proliferation and invasiveness was already observable at 18 h. This could indicate that the oncogenic Ras protein, which is spontaneously activated on the MDA-MB-231 cell membrane, is probably independent of FPP control.

Thus, the participation of Ras could be considered as a subsidiary mechanism for the anti-proliferative and anti-invasive properties of cerivastatin on MDA-MB-231 cells.

As NFκB is involved in regulating the expression of genes required for cell invasiveness, especially protease expression, which allows cells to migrate by degrading components of the extracellular matrix, we also investigated the effects of cerivastatin treatment on u-PA expression and MMP-9 secretion. An inhibitory effect of cerivastatin on u-PA and MMP-9 expression was demonstrated, but it was moderate and lower than that expected from the inhibitory effect on cell invasiveness. Furthermore, it needed 36 h incubation with cerivastatin, while inhibition of cell invasiveness was observed from 18 h. This delayed effect on u-PA expression in comparison with NFκB could be explained by the time required for u-PA clearance in these cells (41). In contrast, the inhibitory effect of cerivastatin on TF expression (a protein also involved in cell invasiveness) is more intense and is evident from 18 h. This decrease is shown by both decreases in mRNA and protein expression on the cell surface. The differences in the kinetic of modification of u-PA and TF by cerivastatin could be due to the fact that AP-1 is the major regulator of TF (42) and AP-1 transcription is dependent on prenylated RhoA (10). Therefore, the early decrease in TF expression could be related to AP-1 inhibition rather than inhibition of NFκB. This hypothesis is supported by the experiments with MG-132, which did not decrease TF. This inhibition of TF expression could contribute to a decrease in cell invasiveness and also a decrease in thrombotic risk.

Obviously, the decrease in u-PA and MMP-9 expression induced by cerivastatin seems unlikely to be the only mechanism involved in inhibition of MDA-MB-231 cell invasiveness. An additional mechanism by which cerivastatin could confer its anti-invasive effect could be considered on the basis of the relationship between Rho GTPases and the actin cytoskeleton. Indeed, recent evidence has strongly suggested the involvement of Rho GTPases in carcinoma cell migration and invasion (43,44). In addition, numerous studies have highlighted the importance of RhoA in the regulation of signaling pathways that mediate the distinct actin cytoskeleton changes required for both cell motility and cell–cell adhesion (9). The deactivation of RhoA induced by cerivastatin could explain the diminished motility of MDA-MB-231 cells. This hypothesis is strengthened by the observation of a parallel decrease in cell membrane-associated RhoA and the disappearance of actin stress fibers, as shown by confocal microscopy. This effect on RhoA inhibition is in agreement with the observation that addition of GGPP completely inhibits the morphological changes associated with the decreased motility of MDA-MB-231 cells induced by cerivastatin, while the action of FPP is low. This relationship between a decrease in Rho signaling and a decrease in cell migration is in agreement with a recent report showing that a Rho kinase inhibitor retards invasive progress of cancer cells (45).

These mechanisms of cerivastatin action could explain why the effect of cerivastatin is cell dependent, acting mostly on aggressive cells where RhoA is overexpressed, while MCF-7 breast cancer cells were only poorly affected by cerivastatin up to 25 ng/ml; cerivastatin did not induce an inhibitory effect on MCF-7 cell proliferation. Moreover, its effect on cell detachment is weak and requires a long incubation period. In addition, cerivastatin induces neither a reduction in u-PA and TF expression nor cell shape changes in MCF-7 cells.

In conclusion, cerivastatin was shown to mainly inhibit RhoA cell signaling pathways involved in the invasiveness and metastatic properties of highly invasive cancer cells. This therefore suggests that cerivastatin could offer a novel approach in the therapy of aggressive forms of cancer in combination with other anti-cancer treatments.

Acknowledgements

The authors thank Dr Bernard Lenormand (CHU Charles Nicolle, Rouen) for his help with the flow cytometry, Elisabeth Legrand and Marianne Paresy for their excellent technical assistance and Richard Medeiros for his advice on editing the manuscript. We are grateful to Drs Hilmar Bischoff (Bayer Germany) and Antoine Chartier (Bayer France), who provided cerivastatin. C.D. is the recipient of a fellowship from the Conseil Régional de Haute Normandie. This study was supported by grants from le Groupement des Entreprises Françaises dans la Lutte contre le Cancer (GEFLUC), la Ligue Régionale de Haute de Normandie and l'Association Régionale pour l'Enseignement et la Recherche Scientifique Technologique (ARERS) and l'Association pour la Recherche sur le Cancer (ARC) (M.K.).

References

1. Bellosta,S., Ferri,N., Bernini,F., Paoletti,R. and Corsini,A. (2000) Non-lipid-related effects of statins. *Ann. Med.*, **32**, 164–176.
2. Matar,P., Rozados,V.R., Roggero,E.A. and Scharovsky,O.G. (1998) Lovastatin inhibits tumor growth and metastasis development of a rat fibrosarcoma. *Cancer Biother. Radiopharm.*, **13**, 387–393.
3. Pedersen,T.R., Wilhelmsen,L., Faergeman,O., Strandberg,T.E., Thorgeirsson,G., Troedson,L., Kristianson,J., Berg,K., Cook,T.J., Haghfelt,T., Kjekshus,J., Miettinen,T., Olsonn,A.G., Pyorala,K. and Wedel,H. (2000) Follow-up study of patients randomized in the Scandinavian simvastatin survival study (4S) of cholesterol lowering. *Am. J. Cardiol.*, **86**, 257–262.
4. Campbell,S.L., Khosravi-Far,R., Rossman,K.L., Clark,G.J. and Der,C.J. (1998) Increasing complexity of Ras signaling (Review). *Oncogene*, **17**, 1395–1413.
5. Yoshioka,K., Nakamori,S. and Itoh,K. (1999) Overexpression of small GTP-binding protein RhoA promotes invasion of tumor cells. *Cancer Res.*, **59**, 2004–2010.

6. Kozma,S.C., Bogaard,M.E., Buser,K., Saurer,S.M., Bos,J.L., Groner,B. and Hynes,N.E. (1987) The human c-Kirsten ras gene is activated by a novel mutation in codon 13 in the breast carcinoma cell line MDA-MB-231. *Nucleic Acids Res.*, **15**, 5963–5971.
7. Fritz,G., Just,I. and Kaina,B. (1999) Rho GTPases are over-expressed in human tumors. *Int. J. Cancer*, **81**, 682–687.
8. Allal,C., Favre,G., Couderc,B., Salicio,S., Sixou,S., Hamilton,A.D., Sebti,S.M., Lajoie-Mazenc,I. and Pradines,A. (2000) RhoA prenylation is required for promotion of cell growth and transformation, cytoskeleton organization, but not for induction of SRE transcription. *J. Biol. Chem.*, **275**, 31001–31008.
9. Takaishi,K., Kikuchi,A., Kuroda,S., Kotani,K., Sasaki,T. and Takai,Y. (1993) Involvement of rho p21 and its inhibitory GDP/GTP exchange protein (rho-GDI) in cell motility. *Mol. Cell. Biol.*, **13**, 72–79.
10. Chang,J.H., Pratt,J.C., Sawasdikosol,S., Kapeller,R. and Burakoff,S.J. (1998) The small GTP-binding protein Rho potentiates AP-1 transcription in T cells. *Mol. Cell. Biol.*, **18**, 4986–4993.
11. Lewis,T.S., Shapiro,P.S. and Ahn,N.G. (1998) Signal transduction through MAP kinase cascades (Review). *Adv. Cancer Res.*, **74**, 49–139.
12. Perona,R., Montaner,S., Saniger,L., Sanchez-Perez,I., Bravo,R. and Lacal,J.C. (1997) Activation of the nuclear factor-kappaB by Rho, CDC42, and Rac-1 proteins. *Genes Dev.*, **11**, 463–475.
13. Finco,T.S. and Baldwin,A.S.Jr (1993) Kappa B site-dependent induction of gene expression by diverse inducers of nuclear factor kappa B requires Raf-1. *J. Biol. Chem.*, **268**, 17676–17679.
14. Nakshatri,H., Bhat- Nakshatri,P., Martin,D.A., Goulet,R.J. and Sledge,G.W. (1997) Constitutive activation of NF-κB during progression of breast cancer to hormone-independent growth. *Mol. Cell. Biol.*, **17**, 3629–3639.
15. Hansen,S.K., Nerlov,C., Zabel,U., Verde,P., Johnsen,M., Baeuerle,P.A. and Blasi,F. (1992) A novel complex between the p65 subunit of NF-κB and c-Rel binds to a DNA element involved in the phorbol ester induction of the human urokinase gene. *EMBO J.*, **11**, 205–213.
16. Mackman,N. (1997) Regulation of the tissue factor gene. *Thromb. Haemost.*, **78**, 747–754.
17. Bond,M., Fabunmi,R.P., Baker,A.H. and Newby,A.C. (1998) Synergistic up-regulation of metalloproteinase-9 by growth factors and inflammatory cytokines: an absolute requirement for transcription factor NF-Kappa B. *FEBS Lett.*, **435**, 29–34.
18. Duffy,M.J., Duggan,C., MaguireE,T., Mulcahy,K., Elvin,P., McDermott,P., Fennelly,J.J. and O'Higgins,N. (1996) Urokinase plasminogen activator as a predictor of aggressive disease in breast cancer. *Enzyme Protein*, **49**, 85–93.
19. Schmitt,M., Harbeck,N., Thomssen,C., Wilhelm,O., Magdolen,V., Reuning,U., Ulm,K., Höfler,H., Jänicke,F. and Graeff,H. (1997) Clinical impact of the plasminogen activation system in tumour invasion and metastasis: prognostic relevance and target for therapy. *Thromb. Haemost.*, **78**, 285–296.
20. Blasi,F. (1999) Proteolysis, cell adhesion, chemotaxis, and invasiveness are regulated by the u-PA-u-PAR-PAI-1 system (Review). *Thromb. Haemost.*, **82**, 298–304.
21. Ruf,W. and Mueller,B.M. (1996) Tissue factor in cancer angiogenesis and metastasis. *Curr. Opin. Hematol.*, **3**, 379–384.
22. Van Antwerp,D.J., Martin,S.J., Kafri,T., Green,D.R. and Verma,I.M. (1996) Suppression of TNF-α induced apoptosis by NF-κB. *Science*, **274**, 787–789.
23. Beg,A.A. and Baltimore,D. (1996) An essential role for NF-κB in preventing TNF-α induced cell death. *Science*, **274**, 782–784.
24. Whang,C.Y., Mayo,M.W. and Baldwin,A.S.Jr (1996) TNF-α and cancer therapy-induced apoptosis: potentiation by inhibition of NF-κB. *Science*, **274**, 784–787.
25. Vindelov,L.L. and Christensen,I.J. (1990) A review of techniques and results obtained in one laboratory by an integrated system of methods designed for routine clinical flow cytometric DNA analysis. *Cytometry*, **11**, 753–770.
26. Feuillard,J., Gouy,H., Bismuth,G., Lee,L.M., Debre,P. and Korner,M. (1991) NF-κB activation by tumor necrosis factor α in the Jurkat T cell line is independent of protein kinase A, protein kinase C, and Ca^{2+}-regulated kinases. *Cytokine*, **3**, 257–265.
27. Bradford,M.M. (1976) A rapid and sensitive method for the quantification of microgram quantities of protein utilizing the principle of protein dye binding. *Anal. Biochem.*, **72**, 248–254.
28. Garcia,J.A., Wu,F.K., Mitsuyasu,R. and Gaynor,R.B. (1987) Interactions of cellular proteins involved in the transcriptional regulation of the human immunodeficiency virus. *EMBO J.*, **6**, 3761–3770.
29. Korner,M., Harel-Bellan,A., Brini,A.T. and Farrar,W.L. (1990) Characterization of the human immunodeficiency virus type 1 enhancer-binding proteins from the human T-cell line Jurkat. *Biochem. J.*, **265**, 547–554.
30. Jaffray,E., Wood,K.M. and Hay,R.T. (1995) Domain organization of IκB and sites of interaction with NF-κB p65. *Mol. Cell. Biol.*, **15**, 2166–2172.
31. Gingras,D., Gauthier,F., Lamy,S., Desrosiers,R.R. and Beliveau,R. (1998) Localization of RhoA GTPase to endothelial caveolae-enriched membrane domains. *Biochem. Biophys. Res. Commun.*, **247**, 888–893.
32. Harris,J.R., Lippman,M.E., Veronesi,U. and Willett,W. (1992) Breast cancer (1). *N. Engl. J. Med.*, **327**, 319–328.
33. Paterson,H.F., Self,A.J., Garrett,M.D., Just,J., Aktories,K. and Hall,A. (1990) Microinjection of recombinant p21rho induces rapid changes in cell morphology. *J. Cell Biol.*, **111**, 1001–1007.
34. Olson,M.F., Ashworth,A. and Hall,A. (1995) An essential role for Rho, Rac, and Cdc42 GTPases in cell cycle progression through G_1. *Science*, **269**, 1270–1272.
35. Chou,M.M. and Blenis,J. (1996) The 70 kDa S6 kinase complexes with and is activated by the Rho family G proteins Cdc42 and Rac1. *Cell*, **85**, 573–583.
36. Perona,R., Esteve,P., Jimenez,B., Ballestero,R.P., Ramon y Cajal,S. and Lacal,J.C. (1993) Tumorigenic activity of rho genes from *Aplysia californica*. *Oncogene*, **8**, 1285–1292.
37. Khosravi-Far,R., Solski,P.A., Clark,G.J., Kinch,M.S. and Der,C.J. (1995) Activation of Rac1, RhoA, and mitogen-activated protein kinases is required for Ras transformation. *Mol. Cell. Biol.*, **15**, 6443–6453.
38. Prendergast,G.C., Khosravi-Far,R., Solski,P.A., Kurzawa,H., Lebowitz,P.F. and Der,C.J. (1995) Critical role of Rho in cell transformation by oncogenic Ras. *Oncogene*, **10**, 2289–2296.
39. Gray-Bablin,J., Rao,S. and Keyomarsi,K. (1997) Lovastatin induction of cyclin-dependent kinase inhibitors in human breast cells occurs in a cell cycle-independent fashion. *Cancer Res.*, **57**, 604–609.
40. Palombella,V.J., Rando,O.J., Goldberg,A.L. and Maniatis,T. (1994) The ubiquitin-proteasome pathway is required for processing the NF-kappa B1 precursor protein and the activation of NF-Kappa B. *Cell*, **78**, 773–785.
41. Herz,J., Clouthier,D. and Hammer,R.E. (1992) LDL receptor related protein internalizes and degrades u-PA-PAI-1 complexes is essential for embryo implantation. *Cell*, **71**, 411–421.
42. Zhou,J.N., Ljungdahl,S., Shoshan,M.C., Swedenborg,J. and Linder,S. (1998) Activation of tissue-factor gene expression in breast carcinoma by stimulation of the RAF-ERK signaling pathway. *Mol. Carcinog.*, **21**, 234–243.
43. Yoshioka,K., Matsumura,F., Akedo,H. and Itoh,K. (1998) Small GTP-binding protein Rho stimulates the actomyosin system, leading to invasion of tumor cells. *J. Biol. Chem.*, **273**, 5146–5154.
44. Itoh,K., Yoshioka,K., Akedo,H., Uehata,M., Ishizaki,T. and Narumiya,S. (1999) An essential part for Rho-associated kinase in the transcellular invasion of tumor cells. *Nature Med.*, **5**, 221–225.
45. Somlyo,A.V., Bradshaw,D., Ramos,S., Murphy,C., Myers,C.E. and Somlyo,A.P. (2000) Rho-kinase inhibitor retards migration and *in vivo* dissemination of human prostate cancer cells. *Biochem. Biophys Res. Commun.*, **269**, 652–659.

Received September 7, 2000; revised February 22, 2001; accepted April 17, 2001